Technische Universität Darmstadt
Fachbereich Physik
Institut für Kernphysik
Theoriezentrum
Schlossgartenstrasse 2
64289 Darmstadt, Germany

TECHNISCHE
UNIVERSITÄT
DARMSTADT

BACHELOR-THESIS

Tidal Love Numbers and the I-Love-Relations of Second Family Compact Stars

Daniel Henrik Nevermann

March 25, 2019

Supervisor:
Priv.-Doz. Dr. Michael Buballa
Martin Steil, M.Sc.

Tidale Love'sche Zahlen und die I-Love-Relationen von kompakten Sternen der zweiten Generation
Tidal Love Numbers and the I-Love-Relations of Second Family Compact Stars

Vorgelegte Bachelor-Thesis von Daniel Henrik Nevermann

1. Gutachten: Priv.-Doz. Dr. Michael Buballa
2. Gutachten: Martin Steil, M.Sc.

Tag der Einreichung:

Erklärung zur Bachleor-Thesis

Hiermit versichere ich, Daniel Henrik Nevermann, die vorliegende Bachelor-Thesis gemäß §22 Abs. 7 APB der TU Darmstadt ohne Hilfe Dritter und nur mit den angegebenen Quellen und Hilfsmitteln angefertigt zu haben. Alle Stellen, die Quellen entnommen wurden, sind als solche kenntlich gemacht worden. Diese Arbeit hat in gleicher oder ähnlicher Form noch keiner Prüfungsbehörde vorgelegen.

Mir ist bekannt, dass im Falle eines Plagiats (§38 Abs.2 APB) ein Täuschungsversuch vorliegt, der dazu führt, dass die Arbeit mit 5,0 bewertet und damit ein Prüfungsversuch verbraucht wird. Abschlussarbeiten dürfen nur einmal wiederholt werden.

Bei der abgegebenen Thesis stimmen die schriftliche und die zur Archivierung eingereichte elektronische Fassung gemäß §23 Abs. 7 APB überein.

Darmstadt, den 25. März 2019

_____

(Daniel Henrik Nevermann)

Abstract

In this thesis we will derive and calculate the moment of inertia and the Tidal Love Number of neutron stars. The Tidal Love Number is a quantity that characterizes how easy, or difficult, a companion star could deform the star away from sphericity. In order to do that we first introduce the Tolman-Oppenheimer-Volkoff Equations that arise from the General Theory of Relativity. Then these equations will be solved which will among other things yield mass-radius curves. The matter inside a neutron star is characterized by an Equation of State. Different Equations of State will be discussed and used for the computation of the quantities mentioned above. Finally we will discuss universal relations between the moment of inertia and the Tidal Love Number.

Zusammenfassung

In dieser Arbeit werden wir das Tägheitsmoment und die Tidale Love'sche Zahl für Neutronensterne herleiten und berechnen. Die Love'sche Zahl charakterisiert, wie schwer oder leicht ein zweiter Stern den Stern aus seiner Kugelform deformieren kann. Für diese Berechnungen werden wir zunächst die Tolman-Oppenheimer-Volkoff Gleichungen einführen, welche aus der Allgemeinen Relativitätstheorie hervorgehen. Die Lösung dieser Gleichungen wird uns unter anderem zu Masse-Radius-Kurven führen. Die Materie im Inneren des Sterns ist parametrisiert durch eine Zustandsgleichung. Wir werden verschiedene Zustandsgleichungen diskutieren und diese zur Bestimmung der oben erwähnten Größen nutzen. Schließlich werden wir Universalrelationen zwischen dem Trägheitsmoment und der Tidalen Love'schen Zahl diskutieren.

Contents

Chapter 1

Introduction and Motivation

A key challenge of current high energy physics research is to explore the properties of nuclear matter at very high densities. On the experimental side, particle accelerators are designed to produce high densities. Neutron stars (NS), with their high central density, are a perfect place to research nuclear matter at very high densities in a natural environment.
Neutron stars are compact objects of very high density that have masses of around 1.5 $M_\odot$[1] but radii that are 10^5 times smaller than the suns radius. They therefore present a perfect environment to study nuclear matter properties at very high densities. Densities inside the core can be as high as several times the density that is reached inside heavy atomic nuclei [1].
The Equation of State (EoS) describes the matter inside the star. As there are many different approaches for describing the matter inside the star there are many different EoS. NS are a perfect test field to probe these EoS in extreme conditions. In this work two types of EoS will be used: polytropic EoS and tabulated, realistic EoS. The polytropic EoS are analytical approximations of realistic EoS. We will observe, however that they behave differently when compared to the realistic EoS.
Recently, the Advanced LIGO and Advanced Virgo gravitational-wave detectors made their first observation of a binary NS inspiral [2]. The internal structure of a star influences the waveform, among other quantities characterized by the Tidal Deformability which measures the star's quadrupole deformation in response to a companion's perturbing tidal field [3]. The Tidal Love Number characterizes how easy or difficult it would be to deform a NS away from sphericity [4]. The LIGO observations lead to experimental insight to the Tidal Love Number [2]. Further observations of gravitational waves could be used to extract more information about the EoS [4].
The so called I-Love-Relations [4] are universal relations between the moment of inertia of a slowly rotating star and the Tidal Love Number. These relations are essentially independent of the EoS [4]. In experimental astrophysics these relations allow to measure only the moment of inertia and automatically receive information about the Tidal Love Number and vice versa, even if the Love Number was not easily accessible from an experimental point of view [4].
The study of NS can also be beneficial in fundamental physics. As NS produce very strong gravitational fields, much stronger than observed in our solar system, they are a perfect test to the General Theory of Relativity [4]. Such tests can be found in e.g. [5].
In this work we will discuss properties of the Tidal Love Numbers and the moments of inertia of NS. We will use various EoS and compare the results. Furthermore we will discuss the I-Love-Relations.

The structure of this thesis will be as follows:
First we are going to introduce the theoretical framework of the thesis. We will talk about NS in general and give a short introduction to the necessary concepts of the General Theory of Relativity.

[1] In the following we will refer to the mass of the sun with the symbol $M_\odot$.

The starting point for our NS calculations will be the Tolman-Oppenheimer-Volkoff Equations that will be derived at the end of Chapter 2. These ordinary differential equations (ODE) specify the internal structure of a static, spherically symmetric relativistic NS that consists of a perfect fluid.
In Chapter 3 we will move on to solving the Tolman-Oppenheimer-Volkoff Equations for different EoS. We will present mass-radius-curves that will give an insight to the stability of certain star configurations.
In Chapter 4 we will derive and compute the moment of inertia of a slowly rotating NS. The derivation is done by introducing a perturbation to the metric and solving the interior and exterior gravitational field of a NS in a slowly rotating perturbation [4].
In a similar way the Tidal Love Number can be derived. This will be done in Chapter 5. Furthermore numerical results will be presented for various EoS.
In Chapter 6 we will be using the results obtained from Chapter 4 and 5 and discuss the I-Love-Relations. We will then conclude the thesis with a short summary and give an outlook for further investigation.

Chapter 2

Theoretical Framework

This chapter will introduce the theoretical background of the thesis. First the general properties of neutron stars (NS) will be discussed, then there will be a brief overview of the concepts from General Relativity (GR) which we will use for the calculations in this thesis. We will conclude this chapter with a derivation of the Tolman-Oppenheimer-Volkoff Equations (TOV Equations).

2.1 Introduction to Neutron Stars

Neutron stars are compact stars that contain very high density matter. NS have typical masses of $1.4\,M_\odot$ and radii of around 10 km [1]. In comparison with our sun, NS have similar masses while their radii are 10^5 times smaller than the suns radius. NS are therefore extremely dense objects. The mean mass density can be approximated via

$$\bar{\rho} = \frac{3M_*}{4\pi R_*^3} \approx 7 \cdot 10^{14} \frac{\mathrm{g}}{\mathrm{cm}^3} \approx (2\text{-}3)\rho_0, \tag{2.1}$$

where $\rho_0 = 2.8 \cdot 10^{14}\ \mathrm{g}/\mathrm{cm}^3$ is the normal nuclear mass density [1]. Inside the core, the density can even reach several ρ_0.

2.1.1 Structure of Neutron Stars

A NS is normally divided into five layers. The atmosphere, the outer crust, the inner crust and the outer and inner core (see. Fig. 2.1). The core of the star constitutes most of the star's mass. The following discussion is based on [1].

The thickness of the atmosphere can vary between around 10 centimeters and a couple millimeters. It consists of hot plasma. In the atmosphere, the radiation that the star emits is formed. From observing the radiation, one can get insight to the radius and the mass of the star. For very cold NS a solid or liquid surface is possible.

The outer crust is a few 100 meters thick and reaches up to a density of around $4 \cdot 10^{11}\ \mathrm{g}/\mathrm{cm}^3$. It mostly consists of iron ions and electrons. The electron Fermi energy grows with increased pressure. Trough beta captures the nuclei are enriched with neutrons. For the most part the outer crust is solid.

The inner crust that is a couple km thick, reaches up to a density of $0.5\rho_0$. The inner crust consists of free neutrons, electrons and neutron-rich-nuclei. In this layer the pressure is high enough for free

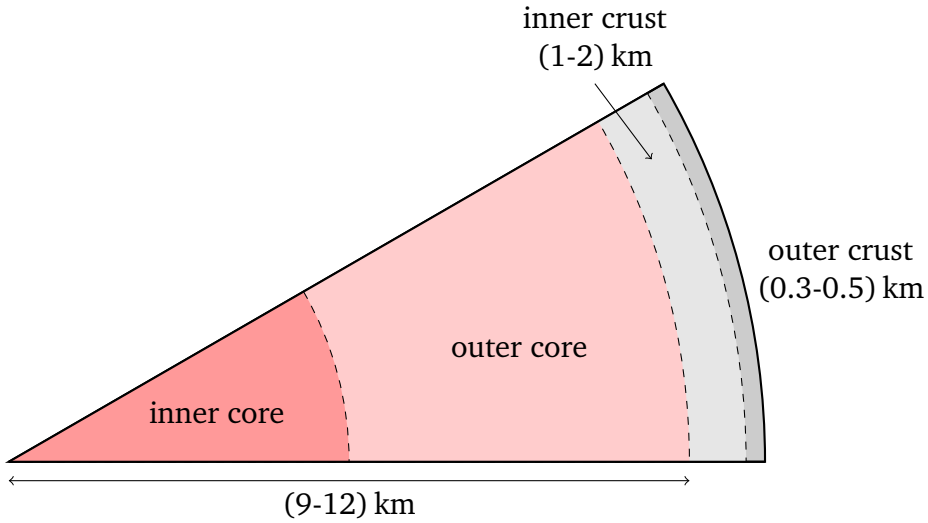

Figure 2.1: Schematic depiction of the NS structure. The thicknesses depends on the model. Created on basis of [1].

neutrons to be stable. The higher the pressure gets, the higher the electron Fermi energy grows. The neutron-rich nuclei begin to release neutrons at a density of around $4.3 \cdot 10^{11}$ g/cm^3 [6].

In the outer core that reaches up to a density of around $2\rho_0$ and extends over several kilometers, the matter mostly consists of free neutrons. Also some protons, electrons and muons are encountered. The components of the $pne\mu$-plasma are strongly degenerate [1]. The protons and neutrons form a strongly interacting, suprafluid Fermi liquid.

The area with higher density than $2\rho_0$ is the inner core. Near the center of the star densities of several ρ_0 are possible. The inner core is several kilometers thick. Especially this layer is not very well understood, as densities are so high that they have not been reproduced on earth. Multiple different exotic matter states have been predicted for this layer. The matter is strongly interacting.

2.2 General Relativity

The so called General Theory of Relativity was outlined by *A. Einstein* and was published 1915 in several papers [7, 8, 9]. GR is the generalization of the Special Theory of Relativity (SR) and describes gravitation via geometric properties of a curved spacetime. GR is the basis for describing compact objects, such as neutron stars and black holes (BH) and predicts the existence of gravitational waves. (cf. [10])

Throughout this work we will use the metric convention $(+,-,-,-)$, furthermore the Einstein summation convention (summation over contracted indices) is implied everywhere. To simplify equations, the gravitational constant G as well as the speed of light c is set to unity (gravitational units).

2.2.1 Mathematical Formalism behind the General Theory of Relativity

The General Theory of Relativity is described on a four dimensional Riemannian manifold. The underlying mathematics of GR is Differential Geometry.
Just like in SR, the points in this space are denoted by **four-vectors**

$$x^\mu = (x^0, x^1, x^2, x^3) \equiv (t, \boldsymbol{x}). \tag{2.2}$$

The displacement between two points is described by a displacement vector $\mathrm{d}x^\mu$. From the chain rule of partial differentiation follows that the displacement vector transforms to arbitrary coordinates x'^μ as

$$\mathrm{d}x'^\mu = \frac{\partial x'^\mu}{\partial x^\nu}\,\mathrm{d}x^\nu. \tag{2.3}$$

A vector that transforms in the same way as the displacement vector is called **contravariant** and is denoted by an upper index. To lower the index one uses the metric tensor $g_{\mu\nu}$

$$A_\mu = g_{\mu\nu}A^\nu. \tag{2.4}$$

A vector with lowered index is called **covariant**. Raising indices works analogously using the metric tensor $A^\mu = g^{\mu\nu}A_\nu$. The transformation law for covariant vectors

$$A'_\mu = \frac{\partial x^\nu}{\partial x'^\mu}A_\nu \tag{2.5}$$

under the change of coordinates is similar to the one for contravariant vectors. In a freely falling reference frame the coordinates are denoted by ξ^μ. The invariant proper time interval $\mathrm{d}\tau^2$ can be expressed using the metric tensor.

$$\mathrm{d}\tau^2 = g_{\mu\nu}\,\mathrm{d}x^\mu\,\mathrm{d}x^\nu = \eta_{\alpha\beta}\,\mathrm{d}\xi^\alpha\,\mathrm{d}\xi^\beta \tag{2.6}$$

Applying (2.3) to the equation above yields a relation between the Minkowski metric $\eta_{\mu\nu}$, known from SR, and the metric tensor.

$$g_{\mu\nu} = \frac{\partial \xi^\alpha}{\partial x^\mu}\frac{\partial \xi^\beta}{\partial x^\nu}\eta_{\alpha\beta}. \tag{2.7}$$

2.2.2 Geodesics and the Christoffel Symbol

One cornerstone of GR is the **equivalence principle**. The weak equivalence principle, that was already hinted by experiments performed by *G. Galilei*, states that the gravitational mass and the inertial mass are equal. Einstein extended this to the statement that in any arbitrary gravitational field, a local inertial frame can be chosen, so that the laws of physics take on the form they have in SR [11]. This extension is called strong equivalence principle. The power of the equivalence principle is that a law that holds in SR, can be generalized to a law that holds within a gravitational field, simply by applying a coordinate transformation.
The equation of motion of a body that is freely falling in an arbitrary gravitational field can be expressed easily in the coordinates of the freely falling inertial frame ξ^α by

$$\frac{\mathrm{d}^2\xi^\alpha}{\mathrm{d}\tau^2} = 0 \tag{2.8}$$

To obtain a connection between the freely falling frame and an arbitrary coordinate system one can use the transformation law (2.3):

$$\frac{\mathrm{d}^2\xi^\alpha}{\mathrm{d}\tau^2} = \frac{\mathrm{d}}{\mathrm{d}\tau}\left[\frac{\partial\xi^\alpha}{\partial x^\mu}\frac{\mathrm{d}x^\mu}{\mathrm{d}\tau}\right] = 0 \tag{2.9a}$$

$$\Leftrightarrow \quad \frac{\partial x^\lambda}{\partial\xi^\alpha}\frac{\partial\xi^\alpha}{\partial x^\mu}\frac{\mathrm{d}^2x^\mu}{\mathrm{d}\tau^2} + \frac{\partial^2\xi^\alpha}{\partial x^\mu\partial x^\nu}\frac{\partial x^\lambda}{\partial\xi^\alpha}\frac{\mathrm{d}x^\mu}{\mathrm{d}\tau}\frac{\mathrm{d}x^\nu}{\mathrm{d}\tau} = 0 \tag{2.9b}$$

$$\overset{\text{def.}}{\Leftrightarrow} \quad \frac{\mathrm{d}^2x^\lambda}{\mathrm{d}\tau^2} + \Gamma^\lambda_{\mu\nu}\frac{\mathrm{d}x^\mu}{\mathrm{d}\tau}\frac{\mathrm{d}x^\nu}{\mathrm{d}\tau} = 0. \tag{2.9c}$$

In the second line we carried out the chain rule and multiplied by $\partial x^\lambda \big/ \partial\xi^\alpha$. The last line in this equation (2.9c) defines the **Christoffel Symbol**[1] $\Gamma^\lambda_{\mu\nu}$. The path defined by this equation is called a **geodesic**. Within the Lagrangian formalism it can be shown that this path extremizes the proper time (e.g. see [11]).
The Christoffel Symbol can also be expressed in terms of the metric tensor:

$$\Gamma^\lambda_{\mu\nu} = \frac{1}{2}g^{\lambda\kappa}\left(\frac{\partial g_{\kappa\nu}}{\partial x^\mu} + \frac{\partial g_{\kappa\mu}}{\partial x^\nu} - \frac{\partial g_{\mu\nu}}{\partial x^\kappa}\right). \tag{2.10}$$

The Christoffel Symbol is symmetric in its lower two indices.

2.2.3 Riemann Curvature Tensor and the Einstein Field Equations

One important consequence of the equivalence principle, introduced in the last section, is the **principle of covariance**. As physical laws must be independent of the chosen coordinates, there are two important requirements to any law that holds in a gravitational field. Firstly any equation that holds in a gravitational field, must be covariant under any coordinate transformation (i.e. maintain its form under any coordinate transformation). Secondly all equations that hold in the presence of a gravitational field must also hold in a local inertial frame (i.e. if the metric tensor is replaced with the Minkowski metric the corresponding law from SR must result). The ordinary derivative however does change its form under coordinate transformation. The ordinary derivative of a vector is a non-tensor. A different type of derivative is required.
In order to keep the equations easy to read, its also useful to introduce a shorthand notation for the ordinary derivative. The **covariant derivative** for a co- and contravariant vector is defined by:

$$\begin{aligned} A_{\mu||\nu} &\equiv A_{\mu|\nu} - \Gamma^\lambda_{\mu\nu}A_\lambda \equiv \frac{\mathrm{d}A_\mu}{\mathrm{d}x^\nu} - \Gamma^\lambda_{\mu\nu}A_\lambda, \\ A^\mu_{||\nu} &\equiv A^\mu_{|\nu} + \Gamma^\mu_{\lambda\nu}A^\lambda \equiv \frac{\mathrm{d}A^\mu}{\mathrm{d}x^\nu} + \Gamma^\mu_{\lambda\nu}A^\lambda. \end{aligned} \tag{2.11}$$

In an inertial frame the Christoffel Symbol vanishes and the covariant derivative equals the ordinary derivative. By applying the chain-rule several times it can be shown that the covariant derivative of a vector $A^\mu_{||\nu}$ in fact does transform as a tensor.
These definitions are sufficient to introduce the **Riemann Curvature Tensor**

$$R^\rho_{\sigma\mu\nu} \equiv \Gamma^\rho_{\sigma\nu|\mu} - \Gamma^\rho_{\sigma\mu|\nu} + \Gamma^\alpha_{\sigma\nu}\Gamma^\rho_{\alpha\mu} - \Gamma^\alpha_{\sigma\mu}\Gamma^\rho_{\alpha\nu} \tag{2.12}$$

[1] Some literature, including [11], calls $\Gamma^\lambda_{\mu\nu}$ the *affine connection*.

If the Riemann Tensor vanishes the space is flat and vice versa. The Riemann Tensor $R^{\rho}_{\sigma\mu\nu}$ is antisymmetric in its last two indices. The symmetric **Ricci Tensor** is defined as the following contraction of indices:

$$R_{\mu\nu} \equiv R^{\alpha}_{\mu\nu\alpha}. \tag{2.13}$$

Furthermore one can define the **Scalar Curvature** $R \equiv g^{\mu\nu}R_{\mu\nu}$. Finally the **Einstein Tensor** can be defined:

$$G^{\mu\nu} \equiv R^{\mu\nu} - \frac{1}{2}g^{\mu\nu}R. \tag{2.14}$$

The Einstein Tensor is divergenceless, i.e. $G^{\mu\nu}_{||\nu} = 0$, and symmetric. The **Einstein Field Equations** now state that the Einstein Tensor is equal to the symmetric and divergenceless tensor $T^{\mu\nu}$:

$$\boxed{G^{\mu\nu} = \kappa T^{\mu\nu},} \tag{2.15}$$

where $T^{\mu\nu}$ is the Energy-Momentum-Tensor. In GR any type of mass or energy contributes equally as a source of curved spacetime. These sources are incorporated into a symmetric, divergenceless second-rank Tensor, the Energy-Momentum-Tensor. Frequently matter can be treated as a perfect fluid. For a perfect fluid the Energy-Momentum-Tensor reads:

$$T^{\mu\nu} = -p g^{\mu\nu} + u^{\mu}u^{\nu}(p + \epsilon), \tag{2.16}$$

where u^{μ} is the local fluid four-velocity $u^{\mu} = \mathrm{d}x^{\mu}/\mathrm{d}\tau$, p is the pressure and ϵ is the energy density. From the Newtonian limit the constant $\kappa = -8\pi$ can be determined.

2.2.4 The Schwarzschild Solution

The easiest region to solve the Einstein Field Equations in is static isotropic space. The most general form of the line element for static isotropic spacetime is

$$\mathrm{d}\tau^2 = \mathcal{B}(r)\,\mathrm{d}t^2 - \mathcal{A}(r)\,\mathrm{d}r^2 - r^2\big(\mathrm{d}\theta^2 + \sin^2\theta\,\mathrm{d}\phi^2\big). \tag{2.17}$$

At infinite distance to any source of gravity (i.e. at $r \to \infty$) the functions $\mathcal{A}(r)$ and $\mathcal{B}(r)$ must converge to unity, in order to fulfill the flat space limit. A substantial ansatz is

$$\mathcal{A}(r) = \exp[2\lambda(r)] \quad \text{and} \quad \mathcal{B}(r) = \exp[2\nu(r)], \tag{2.18}$$

where λ and ν go to zero for large r. Using (2.12) the non-zero components of the Ricci Tensor can be computed:

$$\begin{aligned}
R_{00} &= \left(-\nu'' + \lambda'\nu' - \nu'^2 - \frac{2\nu'}{r}\right)e^{2(\nu-\lambda)},\\
R_{11} &= \nu'' - \lambda'\nu' + \nu'^2 - \frac{2\lambda'}{r},\\
R_{22} &= \big(1 + r\nu' - r\lambda'\big)e^{-2\lambda} - 1,\\
R_{33} &= R_{22}\sin^2\theta.
\end{aligned} \tag{2.19}$$

In empty space the Einstein Field Equations (2.15) reduce to $G^{\mu\nu} = 0$. Shifting one index in this relation yields

$$R^{\alpha}_{\nu} = \frac{1}{2}\delta^{\alpha}_{\nu}R, \tag{2.20}$$

which implies that $R = 2R \Longleftrightarrow R = 0$, after contraction of indices, hence the right side of (2.20) is zero, i.e. $R_{\mu\nu} = 0$. This implies that the bracket in the first line of (2.19) is zero, as well as the second line and therefore $R_{00} + R_{11} = 0$ holds. From that it follows that $\lambda' + \nu' = 0$ holds. Due to the flat space limit $\lambda + \nu = 0$ also must be true. Inserting those results into R_{22} yields

$$(1 + 2r\nu')e^{2\nu} = 1. \tag{2.21}$$

This ODE implies $\exp(2\nu) = 1 - 2M/r$, where M is the mass of the gravitational source. As $\lambda = -\nu$ the metric for static, isotropic space outside a star can be written as

$$\mathrm{d}\tau^2 = \left(1 - \frac{2M}{r}\right)\mathrm{d}t^2 - \left(1 - \frac{2M}{r}\right)^{-1}\mathrm{d}r^2 - r^2\left(\mathrm{d}\theta^2 + \sin^2\theta\,\mathrm{d}\phi^2\right). \tag{2.22}$$

This is the **Schwarzschild Solution** [12].

2.3 Tolman-Oppenheimer-Volkoff Equations

At the end of the last section a solution to the Einstein Field Equations for static isotropic space outside a compact object, the Schwarzschild Solution, was derived. The goal of this section is to derive equations for the structure of a static, spherically symmetric, relativistic star that consists of a perfect fluid.
The vanishing of the Scalar Curvature that was established for empty space does not hold inside a star. Using (2.17) with the ansatz from (2.18) the Scalar Curvature can be derived:

$$R = g^{\mu\nu}R_{\mu\nu} = e^{-2\nu}R_{00} - e^{-2\lambda}R_{11} - \frac{2}{r^2}R_{22}. \tag{2.23}$$

Expressions for $R_{\mu\mu}$ are written out in (2.19). In static stars, the three-velocity vanishes (i.e. $u^{\mu\in\{1,2,3\}} = 0$). The time component of the four-velocity can be derived from the normalization condition ($g_{\mu\nu}u^\mu u^\nu = 1$), resulting in $u^0 = 1/\sqrt{g_{00}}$. Inserting this into (2.16) yields

$$T^{\mu\nu} = \mathrm{diag}\left[e^{-2\nu}\left(p\left(1 - e^{4\nu}\right) + \epsilon\right), -e^{2\lambda}p, -r^2p, -r^2\sin^2\theta\, p\right]. \tag{2.24}$$

Now the Einstein Field Equations can be written out. For convenience, one index is lowered.

$$G_0^0 = e^{-2\lambda}\left(\frac{1}{r^2} - \frac{2\lambda'}{r}\right) - \frac{1}{r^2} = -8\pi\epsilon \tag{2.25a}$$

$$G_1^1 = e^{-2\lambda}\left(\frac{1}{r^2} - \frac{2\nu'}{r}\right) - \frac{1}{r^2} = 8\pi p \tag{2.25b}$$

$$G_2^2 = e^{-2\lambda}\left(\nu'' + \nu'^2 - \lambda'\nu' + \frac{\nu' - \lambda'}{r}\right) = 8\pi p \tag{2.25c}$$

$$G_3^3 = G_2^2 = 8\pi p \tag{2.25d}$$

The equation corresponding to the 00-component of the Einstein Tensor can be rewritten:

$$\frac{\mathrm{d}}{\mathrm{d}r}\left[r\left(1 - e^{-2\lambda(r)}\right)\right] = 8\pi r^2\epsilon(r) \tag{2.26}$$

Integrating both sides of this equation and rearranging the terms yields

$$e^{-2\lambda(r)} = 1 - \frac{8\pi}{r}\int_0^r \mathrm{d}r'\, r'^2 \epsilon(r') \equiv 1 - \frac{2M(r)}{r}, \tag{2.27}$$

where $M(r)$ is the incorporated mass at radius r. At the edge of the star, $M(r = R_*) \equiv M_*$ equals the total mass of the star.
From (2.25a), (2.25b) and (2.27) one can obtain expressions for λ', ν', ν'' and ν'^2 in terms of p, p', ϵ and $M(r)$. Inserting these into (2.25c) and using (2.27) results in the **Tolman-Oppenheimer-Volkoff Equations**:

$$\frac{\mathrm{d}p}{\mathrm{d}r} = -\frac{\big[p(r)+\epsilon(r)\big]\big[M(r)+4\pi r^3 p(r)\big]}{r[r-2M(r)]} \tag{2.28}$$

Together with the equation for the mass that follows from (2.27)

$$M'(r) = 4\pi r^2 \epsilon(r) \tag{2.29}$$

and an **Equation of State** (EoS) that relates the pressure with the energy density they form a coupled ODE system which specifies the structure of the star with a given central pressure $p_c \equiv p(r=0)$ fully.

2.4 Interior Schwarzschild Solution

Besides the solution in empty space, *K. Schwarzschild* also published an analytic solution to the interior of an incompressible fluid sphere, the **Interior Schwarzschild Solution** (ISS) [13].
The assumption here is that the energy density is constant. The mass of the fluid sphere therefore is given by

$$M_* = \frac{4\pi}{3} R_*^3 \epsilon_c \quad \Leftrightarrow \quad \epsilon_c = \frac{3M_*}{4\pi R_*^3} \tag{2.30}$$

with the constant energy density ϵ_c. The equation for the mass (2.29) can now be integrated analytically:

$$M(r) = \frac{4\pi}{3} r^3 \epsilon_c = \frac{M_* r^3}{R_*^3}. \tag{2.31}$$

The equations (2.30) and (2.31) can be inserted into the TOV Equation (2.28):

$$p'(r) = -\frac{r\big[M_* + 4\pi R_*^3 p(r)\big]\big[3M_* + 4\pi R_*^3 p(r)\big]}{4\pi R_*^3\big[R_*^3 - 2M_* r^2\big]}. \tag{2.32}$$

When the edge of the star is reached the pressure should naturally be zero which leads to the initial condition $p(R_*) = 0$. The solution to (2.32) is given by

$$p(r) = -\frac{3M_*\big(\sqrt{r^2(R_*-2M_*)} - \sqrt{R_*^3 - 2M_* r^2}\big)}{4\pi R_*^3\big(3\sqrt{R_*^2(R_*-2M_*)} - \sqrt{R_*^3 - 2M_* r^2}\big)}. \tag{2.33}$$

In Fig. 2.2, the pressure and mass are plotted over the radius for a star with mass $M_* \approx 2.193\, M_\odot$ and radius $R_* \approx 16.787\,\mathrm{km}$. The resulting central pressure is $p(r=0) = p_c = 19.7588\ \mathrm{MeV/fm^3}$.

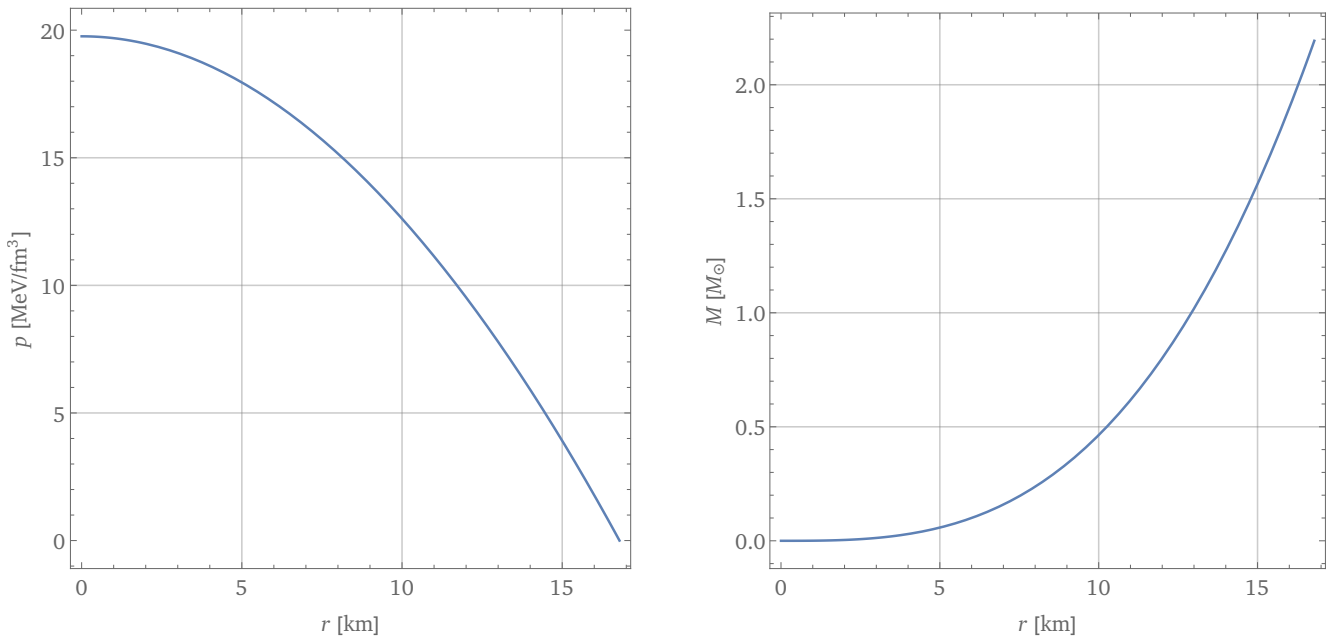

a **b**

Figure 2.2: ISS for a star with mass $M_* \approx 2.193\, M_\odot$ and radius $R_* \approx 16.787\,\text{km}$. The central pressure of the star is $p_c = 19.7588\ \text{MeV}/\text{fm}^3$. The pressure is shown in **a** and the mass in **b**.

From (2.30) the constant energy density ϵ_c for this star is easily calculated to be $123.447\ \text{MeV}/\text{fm}^3$. Although the ISS is not very realistic, the general structure of the solution can be observed. The pressure gradually decreases until the surface of the star is reached while the included mass gradually increases. At the surface, the pressure has decreased to zero, while the mass amounted to the total mass of the star.

Chapter 3

Solving the Tolman-Oppenheimer-Volkoff Equations

In the last section the TOV Equations were derived. The focus of this section is to solve the TOV Equations using various EoS. Besides taking a look at the solutions for the pressure and the mass gradients, the mass-radius-curves are will be calculated.

The solution to the TOV Equations are functions of the pressure p and the mass M in terms of the radius. In general the TOV Equations can not be solved analytically but have to be integrated numerically. We will start the integration in the center of the star and integrate outwards until the pressure is zero. Then the surface of the star is reached. The radius at this point equals the total radius R_* of the star. The total mass of the star is $M_* \equiv M(R_*)$. The central pressure p_c acts as the initial condition. For practical reasons we do not start the integration at $r = 0$ but at an arbitrary small r_0. The central pressure therefore is the value of p at r_0. The mass at r_0 is obtained by fixing the energy density to the central energy density ϵ_c and integrating (2.29).

All calculations in this thesis were done with *Wolfram Mathematica 11*. For the numerical solution of the ODE, the built in routine `NDSolve` was used.

3.1 Gravitational Units

We mentioned at the beginning of Sec. 2.2 that gravitational units will be used in this work. In these units all relevant constants, such as the gravitational constant G and the speed of light c are set to unity. This is useful when dealing with analytic expressions, as equations get easier to read and to handle without having to deal with a lot of constants. Normally the units are changed back to canonical units before calculating anything particular. The conversion factors to canonical units can be obtained by multiplying by matching constants. In the following calculations the units of the constants are put in square brackets.

$$\begin{aligned} 1\,\mathrm{s} &= 1\,\mathrm{s}\cdot c\left[\frac{\mathrm{m}}{\mathrm{s}}\right] = 2.9979\cdot 10^{8}\,\mathrm{m} \\ 1\,\mathrm{kg} &= 1\,\mathrm{kg}\cdot\frac{G\left[\frac{\mathrm{m}^3}{\mathrm{kg\,s}^2}\right]}{c^2\left[\frac{\mathrm{m}^2}{\mathrm{s}^2}\right]} = 7.4237\cdot 10^{-31}\,\mathrm{m} \\ 1\,\mathrm{J} &= 1\,\frac{\mathrm{kg\,m}^2}{\mathrm{s}^2}\cdot\frac{G\left[\frac{\mathrm{m}^3}{\mathrm{kg\,s}^2}\right]}{c^4\left[\frac{\mathrm{m}^4}{\mathrm{s}^4}\right]} = 8.2622\cdot 10^{-45}\,\mathrm{m} \end{aligned} \tag{3.1}$$

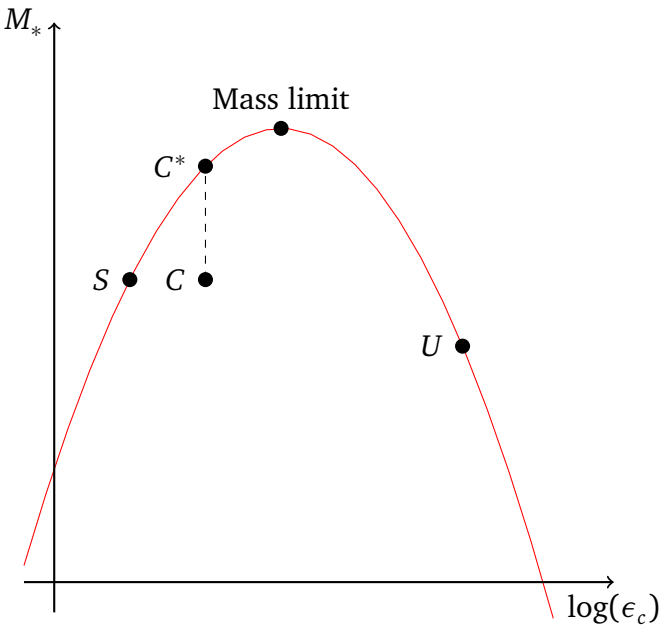

Figure 3.1: Schematic plot of possible solutions to the TOV-Equations around the mass limit point (equilibrium solutions lie on the red line). This illustrates the necessary condition for stability.

A common choice in TOV calculations is to use $\mathrm{MeV}/\mathrm{fm}^3$ for p and ϵ and km for M and r. Using the results from above, one finds the relation between $\mathrm{MeV}/\mathrm{fm}^3$ and km:

$$1\,\frac{\mathrm{MeV}}{\mathrm{fm}^3} = 1.3234 \cdot 10^{-6}\,\frac{1}{\mathrm{km}^2}. \tag{3.2}$$

It will also be practical to specify masses as multiples of the solar mass $M_\odot$. The value of the solar mass in km is $M_\odot = 1.4766\,\mathrm{km}$. (cf. [11])

3.2 Mass-Radius-Curves

Before moving on to more realistic EoS we will talk about **Mass-Radius-Curves**. As mentioned at the beginning of this chapter, the numerical calculations of the TOV Equations with initial pressure p_c, result in values for the total mass and the total radius of the star. When solving the TOV Equations for multiple different values of p_c we obtain multiple different tuples for R_* and M_*. Plotting the masses over the radii results in a mass-radius-curve. Analyzing the mass-radius-curve can give insight to the stability of a star with a certain mass-radius tuple.

3.2.1 Necessary Condition for Stability

In this section we will introduce a necessary but not sufficient condition for the stability of a star [11].
Consider a sequence of equilibrium star configurations around the mass limit as shown in Fig. 3.1. A stable star is in an equilibrium between the gravitational force that acts inwards at the surface

and the force induced by the pressure that is dependent on the EoS. Now consider an arbitrary star S in this sequence. If the energy density of this star is increased due to a perturbation, the star is compressed and displaced to C. At C it is not in an equilibrium configuration anymore. The equilibrium star with the same energy density as C lies at C^*. The star at C hence has a deficit in mass. Gravity therefore under balances the central pressure gradient that increased with the central energy density and pushes the star back to S. A similar argument holds if the star is decompressed. For a star at U that lies on the decreasing part of the curve the situation is different. If this star is perturbed and shifted towards higher energy density, the star with the same energy density, that is in an equilibrium configuration, has a lower total mass. The gravitation is stronger than it would be in equilibrium and over compensates the inner pressure which makes the compression even stronger. The star is unstable. From this argumentation the necessary condition for stability

$$\frac{\partial M_*}{\partial \epsilon_c} > 0 \tag{3.3}$$

arises. A star that lies on the increasing part of the mass-radius-curve fulfills this condition and is stable, while a star that lies on the decreasing part does not fulfill this condition and therefore is unstable.

3.3 Polytropic Equations of State

An important class of analytic EoS are the **polytropes**. A polytropic EoS is of the form $p = Kn^\gamma$, with the nucleon number density n, a polytropic index γ and a constant K. As it is easier to solve the TOV equation in p, the EoS will be inverted. The polytrope that will be used in this work reads [14]

$$\epsilon(p) = m_B n_{B,0}\left(\frac{p}{\kappa m_B n_{B,0}}\right)^{1/\gamma} + \frac{p}{\gamma - 1}, \tag{3.4}$$

where $m_B = 931.192\,\mathrm{MeV}$ [15] is the baryon mass minus the binding energy in a heavy core (Fe), $n_{B,0} = 0.153\,\mathrm{fm}^{-3}$ [11] is the equilibrium of the nucleon number density and κ is a dimensionless coefficient. For a causal ($c_s \leq c$) polytrope, $\gamma \in (1, 2]$ holds [14]. Throughout this work we will fix the coefficient κ to 0.05 and consider different values for γ. In Fig. 3.2 different polytropes are shown. An EoS can be characterized by its stiffness into stiffer or softer EoS with respect to the compressibility of the matter [1]. The polytrope with $\gamma = 2$ is especially stiff, while the polytrope with $\gamma = 3/2$ is softer. As we will see later, the stiffness of a EoS can change the results of mass-radius-curve calculations drastically.

Solution of the Tolman-Oppenheimer-Volkoff Equations

In Sec. 2.4 the Interior Schwarzschild Solution was introduced as an analytical solution to the TOV Equations. For polytropes the TOV Equations must be integrated numerically, as described in the beginning of the chapter. This gives insight to the internal structure of NS. In Fig. 3.3, the pressure and the mass of the star are shown for different central pressures. For the polytrope with $\gamma = 2$, the stable star with maximum mass has a mass of $1.81\,M_\odot$ at a central pressure of $316.23\ \mathrm{MeV}/\mathrm{fm}^3$. The crosses at $p = 0$ in Fig. 3.3 (a) mark the radii of the stars. From this we see that the radius of the star increases with decreasing central pressure. As for the ISS the pressure decreases monotonically from its maximum in the center of the star with increasing radius, while the mass increases with the

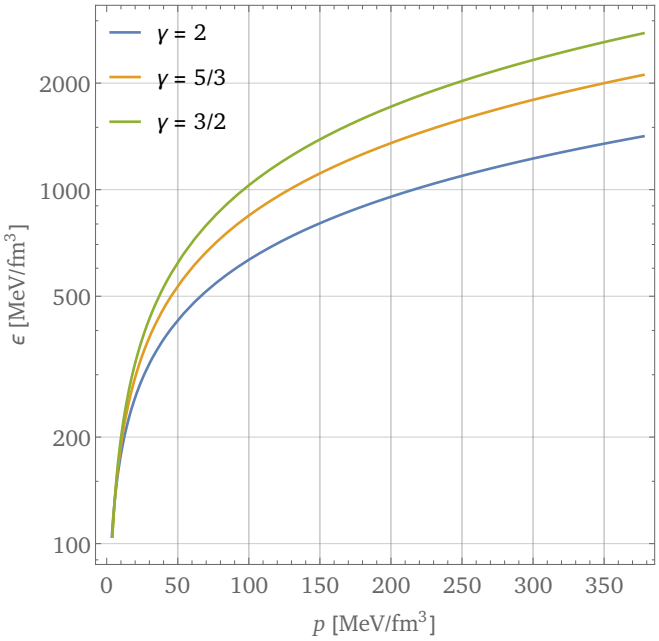

Figure 3.2: Comparison of different polytropes. Higher polytropic indices correspond to stiffer EoS. The polytrope with $\gamma = 2$ is especially stiff.

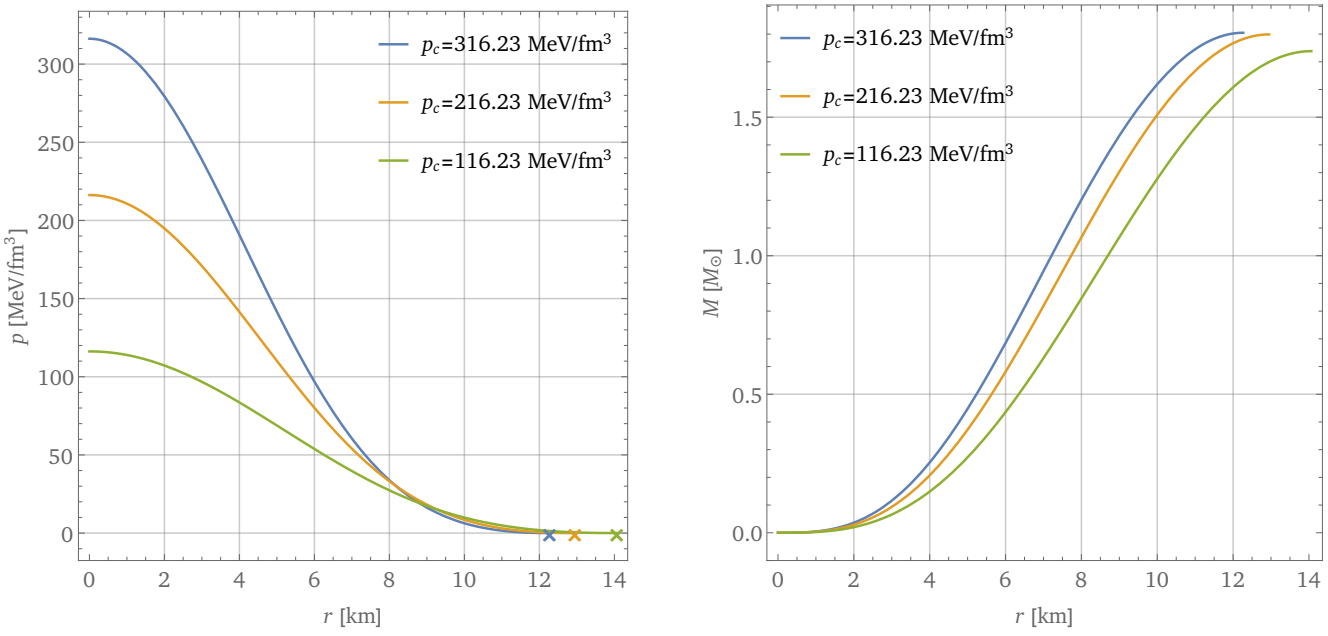

a **b**

Figure 3.3: In **a**, the pressure over the radius and in **b**, the mass over the radius is plotted for three different central pressures and a polytrope with $\gamma = 2$. The star with $p_c = 316.23\ \mathrm{MeV}/\mathrm{fm}^3$ is the one with maximum mass for this EoS. The crosses in **a** mark the radii R_* of the stars.

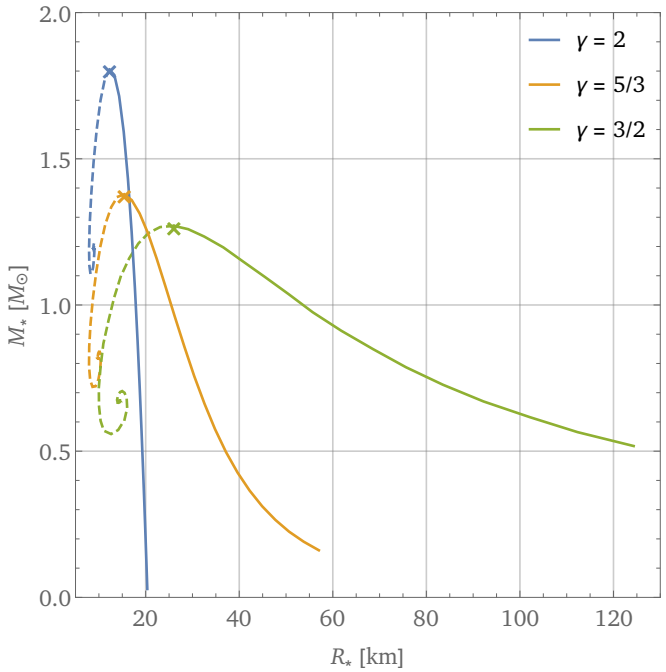

Figure 3.4: Mass-Radius-Curves for different polytropic EoS. The crosses mark the maximum masses. Stars on the dashed part of the curve are unstable.

radius. Near the star's surface, i.e. inside the crust, the pressure decrease is not as steep as inside the core.

Mass-Radius-Curves

The mass-radius-curves for different polytropic EoS are shown in Fig. 3.4. The star with maximum mass for each EoS is marked by a cross. The stars right of the maximum mass star are stable, the ones on the left are unstable. The maximum mass for an EoS decreases with the polytropic index, i.e. stiffer EoS have higher maximum masses, than softer EoS. The difference in maximum mass can reach up to $1\,M_\odot$ between very stiff and very soft EoS [1]. Up to the point were the spiraling starts, the stars in the dashed regions do not fulfill the necessary condition for stability, worked out in the previous section but the stars that lie on the increasing slope of the spiral have $\partial M_*/\partial \epsilon_c > 0$ and are stable, as far as the TOV Equations are concerned. It turns out, however that these stars are also unstable due to unstable vibration modes [16]. Further discussion of the spiraling of the mass-radius-curves of polytropic EoS can be found in [14].

3.4 Realistic Equations of State

The Xtreme Astrophysics Group at the University of Arizona, operates a webpage with realistic, tabulated, up-to-date EoS [17]. Further information can be obtained from their paper [18]. In this work we will consider a couple of the EoS published on [17]: SLY [19], bbb2 [20], WFF2 [21] and AP4 [22]. In Fig. 3.5 these EoS are shown. The bbb2 EoS is especially soft, while the WFF2 is the stiffest of the four. Solving the TOV Equations with the EoS mentioned above for a central pressure of 1000 $\mathrm{MeV}/\mathrm{fm}^3$ yields the curves in Fig. 3.6 (a). The dashed curve is a polytrope with $\gamma = 2$.

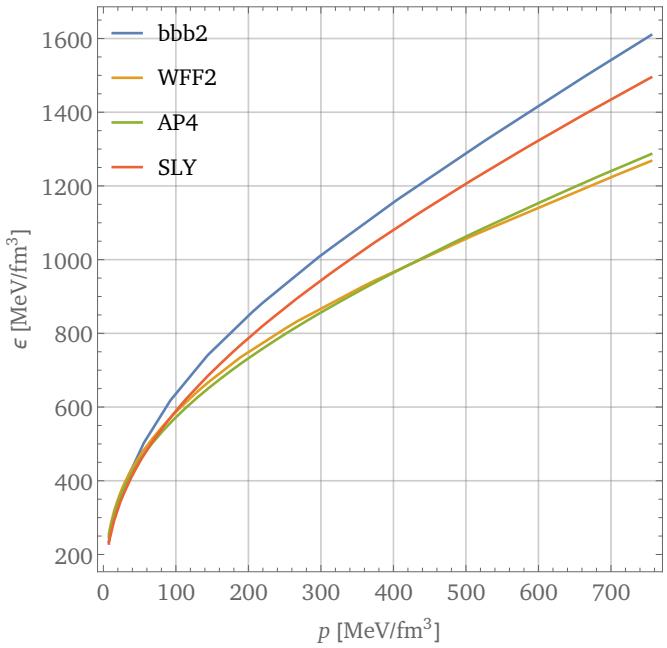

Figure 3.5: Comparison of the different realistic, tabulated EoS. The bbb2 and SLY EoS are softer than the WFF2 and the AP4 EoS.

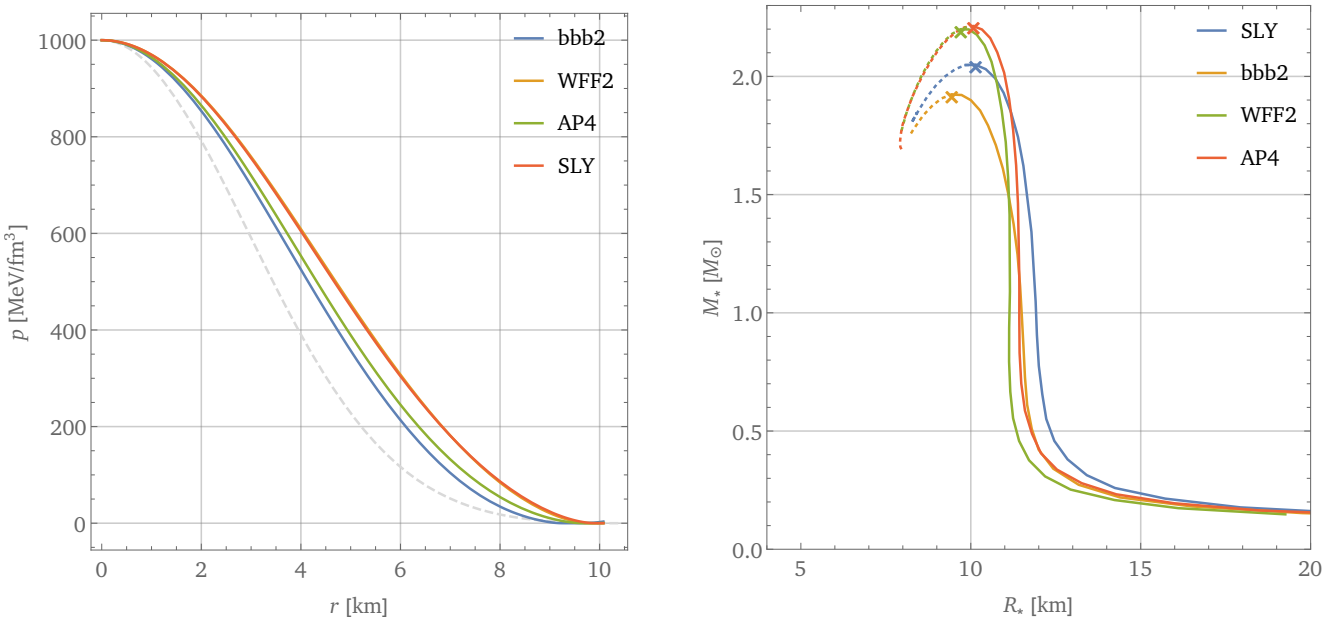

a **b**

Figure 3.6: In **a**, the pressure solution of the TOV Equations is shown. The gray line marks the polytrope with $\gamma = 2$. Note that the star with the polytropic EoS is unstable for this central pressure. In **b**, the Mass-radius-curves for the realistic EoS are shown. The crosses mark the maximum masses.

Compared to the polytrope the realistic EoS have smaller crusts.
The mass-radius-curves are shown in Fig. 3.6 (b). Again we observe that softer EoS have lower maximum masses. The calculated maximum masses match the ones calculated in [17] to about 2%. This deviation is caused most likely by the interpolation method (Hermite interpolation of order 1) of the EoS tables.

Chapter 4

Derivation and Calculation of the Moment of Inertia

In this chapter we consider a slowly rotating, isolated NS up to linear order in its spin. First we are going to derive an expression for the moment of inertia, then numerical results will be presented.

4.1 Derivation of the Moment of Inertia

In order to calculate the moment of inertia I we will introduce a perturbation to the metric. Following [4, 23], the perturbed line element reads:

$$\mathrm{d}\tau^2 = e^{2\nu(r)}\,\mathrm{d}t^2 - e^{2\lambda(r)}\,\mathrm{d}r^2 - r^2\left\{\mathrm{d}\theta^2 + \sin^2\theta[\mathrm{d}\phi - \alpha(\Omega_* - \omega(r))\,\mathrm{d}t]^2\right\}, \tag{4.1}$$

with the perturbation function $\omega(r)$ and the NS angular velocity Ω_*. The parameter α functions as a book-keeping parameter [4]. The order $\mathcal{O}(\alpha^0)$ is solved by the TOV Equations. The effects that we are looking at in this chapter occur at $\mathcal{O}(\alpha^1)$.
Now that the NS is rotating, the three-velocity is no longer zero in all components. The ϕ-component that we chose as the axis of rotation depends on the angular velocity. Following [4], the four-velocity for a slowly rotating star is given by:

$$u^\mu = \left(u^0, 0, 0, \alpha\Omega_* u^0\right). \tag{4.2}$$

From this we can derive the Energy-Momentum-Tensor for a slowly rotating NS by inserting the four-velocity into (2.16). In $\mathcal{O}(\alpha^1)$ the non-zero components read:

$$\begin{aligned} T^0_3 &= -r^2\alpha\sin^2\theta(u^0)^2[p(r)+\epsilon(r)]\omega(r) \\ T^3_0 &= e^{2\nu(r)}\alpha\Omega_*(u^0)^2[p(r)+\epsilon(r)]. \end{aligned} \tag{4.3}$$

Now we can calculate the perturbed Einstein Field Equations. The $(0,3)$-component of these equations is a second order ODE for the perturbation function $\omega(r)$:

$$\omega'' + \omega'\left(4\frac{1-\pi r^2[p+\epsilon]e^{2\lambda}}{r}\right) - \omega\left(16\pi[p+\epsilon]e^{2\lambda}\right) = 0. \tag{4.4}$$

In the literature this equation is frequently referred to as the frame-dragging-equation. In the exterior region of the star the pressure and energy density are zero. This reduces the equation to:

$$\omega'' + 4\frac{\omega'}{r} = 0. \tag{4.5}$$

This equation can be integrated analytically and the integration constants can be identified as the angular velocity and the spin angular momentum J [4, 23]. The exterior solution reads:

$$\omega(r) = \Omega_* - \frac{2J}{r^3} = \Omega_*\left(1 - \frac{2I}{r^3}\right), \tag{4.6}$$

with the definition $I \equiv J/\Omega_*$ of the moment of inertia.
The interior solution can be obtained numerically with the TOV Equations. Before doing that we need to find initial conditions for ω. This is done by inserting the ansatz $\omega(r) = \omega_c(1 + \omega_2 r^2)$ into (4.4) and expanding about the center of the star. From this we eliminate ω_2, so the ansatz only depends on one constant ω_c. This results in an expression for the asymptotic behavior of the interior solution close to the star's center:

$$\omega(r) = \omega_c + \frac{8\pi}{5}(p_c + \epsilon_c)\omega_c r^2 + \mathcal{O}\left(r^3\right) \quad \text{for} \quad r \to 0. \tag{4.7}$$

As (4.4) is arbitrarily scalable, we can choose ω_c arbitrarily to integrate the ODE. Every factor multiplied by this solution will also solve the ODE. We can fix ω_c (and I) by requiring continuity of $\omega(r)$ and its derivative at the star's surface, i.e.

$$\omega^{(\text{int})}(R_*) = \omega^{(\text{ext})}(R_*) \quad \text{and} \quad \omega'^{(\text{int})}(R_*) = \omega'^{(\text{ext})}(R_*). \tag{4.8}$$

The matching condition (4.8) yields the expression

$$\frac{\omega_c}{\Omega_*} = \frac{3}{3\omega(R_*) + R_*\omega'(R_*)} \tag{4.9}$$

for the factor ω_c. With this, we can rescale the numerical solution found by integrating (4.4). The angular velocity has to be specified just like the central pressure, however, for the calculations done here, its value is insignificant. Furthermore the matching condition (4.8) can be solved to give us the expression for the moment of inertia I that we seeked for:

$$I = \frac{R_*^4\omega'(R_*)}{2(R_*\omega'(R_*) + 3\omega(R_*))}. \tag{4.10}$$

4.2 Numerical Results

In the last section we derived an expression for the moment of inertia. In this section we will compute moments of inertia and discuss the results.

In Fig. 4.1 we show the moment of inertia over the compactness C, that is defined as the quotient M_*/R_*, for various EoS. Only stable star configurations are plotted. For the polytrope with polytropic index $\gamma = 2$, the moment of inertia reaches a maximum at a compactness of around 0.15. Up to this value it grows much faster with the compactness than for the realistic EoS. At larger compactness the moment of intertia decreases. As stiffer EoS (AP4, WFF2) have higher maximum masses, they also reach higher values of I.
The moment of inertia divided by the mass times the squared radius of the star over the compactness for various polytropic EoS is shown in Fig. 4.2 (a). Again we see that stiffer EoS have higher values of I than softer EoS. Furthermore the same quantities for the realistic EoS are shown in Fig. 4.2 (b). The polytropes are shown in gray.

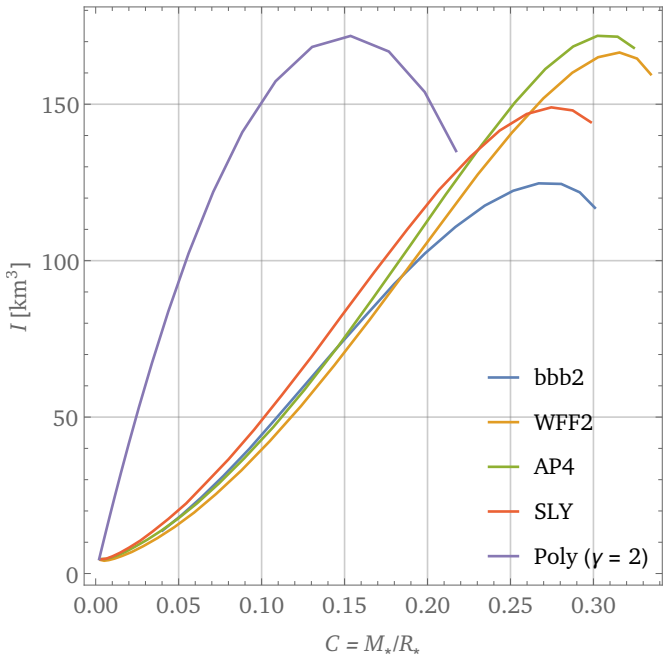

Figure 4.1: Moment of inertia over the compactness for various EoS. Only stable star configurations are plotted.

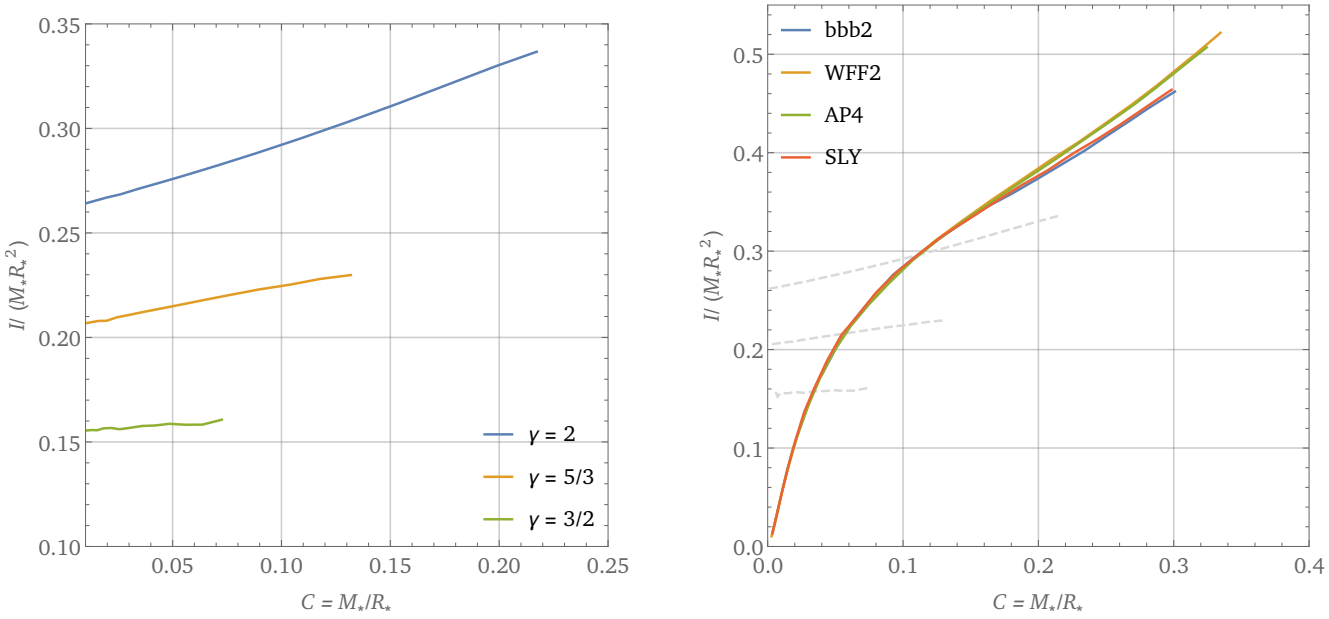

a **b**

Figure 4.2: The moment of inertia divided by the mass times the squared radius of the star over the compactness for polytropic EoS in **a** and for realistic EoS in **b**. In **b**, the polytropic curves are shown in gray. Only stable star configurations are plotted.

Chapter 5

Derivation and Calculation of the Tidal Love Number

Up to this point, we only looked at an isolated star (NS_1). Now we introduce a second companion star (NS_2) and investigate the deformation that this star induces. The aim of this chapter is the derivation of the so called Tidal Love Number. First we are going to work out the necessary definitions, then an expression for the Tidal Love Number is going to be derived. Finally we will present numerical results for the Love Number.

5.1 Definition of the Tidal Love Number

The **Tidal Love Number** characterizes the deformability of a NS away from sphericity [4]. NS_2 induces a tidal quadrupolar tidal field $\mathcal{E}_{ij}$. The static and spherically symmetric NS_1 of mass M_* is placed in this external field and will respond to it by developing a quadrupole moment $\mathcal{Q}_{ij}$. In order for the following calculations to be valid, we need the stars to be far away from each other (i.e. $\text{dist}[NS_1, NS_2] \gg R_*$). In this case the quadrupole moment ($\ell = 2$) dominates over other multipole moments. We introduce the linear response $\lambda_{(\text{tid})}$ by:

$$-\lambda_{(\text{tid})}\mathcal{E}_{ij} \equiv \mathcal{Q}_{ij}, \tag{5.1}$$

where $\mathcal{E}_{ij}$ and $\mathcal{Q}_{ij}$ will be defined as expansion coefficients later. Some literature, including [4], already calls this constant Tidal Love Number. Here we will follow the definitions from [24] and call

$$k_2 \equiv \frac{3}{2}\lambda_{(\text{tid})}R_*^{-5} \tag{5.2}$$

the Tidal Love Number and $\lambda_{(\text{tid})}$ the **Tidal Deformability**. As we will see later, the constant $\lambda_{(\text{tid})}$ is proportional to R_*^5. The Tidal Love Number on the other hand is constructed to be dimensionless. The quadrupole fields $\mathcal{Q}_{ij}$ and $\mathcal{E}_{ij}$ can be expanded in tensor spherical harmonics $\mathcal{Y}_{ij}^{\ell m}$:

$$\begin{aligned}\mathcal{E}_{ij} &= \sum_{m=-2}^{2} \mathcal{E}_m \mathcal{Y}_{ij}^{2m} = \mathcal{E}_0\, \mathcal{Y}_{ij}^{20} \equiv \mathcal{E}\, \mathcal{Y}_{ij}^{20},\\ \mathcal{Q}_{ij} &= \sum_{m=-2}^{2} \mathcal{Q}_m \mathcal{Y}_{ij}^{2m} = \mathcal{Q}_0\, \mathcal{Y}_{ij}^{20} \equiv \mathcal{Q}\, \mathcal{Y}_{ij}^{20}.\end{aligned} \tag{5.3}$$

In the second equality we used that we can orient the coordinate system so that the problem gets symmetric in ϕ. The only component that is non vanishing is the $m = 0$ component. With that we can rewrite (5.1) as follows:

$$\lambda_{(\text{tid})} = -\frac{\mathcal{Q}}{\mathcal{E}}. \tag{5.4}$$

5.2 Derivation of the Tidal Love Number

The derivation of the Tidal Love Number is similar to the derivation of the moment of inertia. Again we introduce a metric perturbation. The perturbed metric we will call $\tilde{g}_{\mu\nu}$. Following [24, 25, 26] we write:

$$\tilde{g}_{\mu\nu} \equiv g_{\mu\nu} + h_{\mu\nu} \equiv g_{\mu\nu} + \mathrm{diag}\left[e^{\nu(r)}\, h_0(r), -e^{\lambda(r)}\, h_2(r), -r^2\, k(r), -r^2 \sin^2\theta\, k(r)\right] \cdot P_2(\cos\theta), \quad (5.5)$$

with perturbation functions $h_0(r), h_2(r)$ and $k(r)$. Furthermore the Energy-Momentum-Tensor is perturbed by a perturbation tensor $\delta T^{\mu\nu}$. The perturbed tensor is defined by

$$\tilde{T}^{\mu}_{\nu} \equiv T^{\mu}_{\nu} + \delta T^{\mu}_{\nu} \equiv T^{\mu}_{\nu} + \mathrm{diag}\left[\delta\epsilon(r,\theta), -\delta p(r,\theta), -\delta p(r,\theta), -\delta p(r,\theta)\right]. \quad (5.6)$$

The perturbation of the energy density can be expressed as $\delta\epsilon = (\mathrm{d}\epsilon/\mathrm{d}p)\delta p$ [24]. With these perturbed quantities we can write down the perturbed Einstein Field Equations

$$\tilde{G}^{\mu}_{\nu} = -8\pi \tilde{T}^{\mu}_{\nu}, \quad (5.7)$$

where the Einstein Tensor $\tilde{G}^{\mu}_{\nu}$ is calculated using the metric $\tilde{g}_{\mu\nu}$. Furthermore we introduce a parameter α into the metric that functions as a book-keeping parameter [4]. At order $\mathcal{O}(\alpha^2)$, the leading-order effects of tidal perturbations occur. The order $\mathcal{O}(\alpha^0)$ is solved by the TOV Equation. To simplify the following equations we will not write down the parameter α, as it only functions as a formal trick.

Deriving a Differential Equation for h_0

The perturbation functions introduced in (5.5) can all be expressed in terms of h_0, resulting in a differential equation for h_0.
We begin by subtracting $\tilde{G}^4_4$ from $\tilde{G}^3_3$:

$$\tilde{G}^3_3 - \tilde{G}^4_4 = -8\pi\left(\tilde{T}^3_3 - \tilde{T}^4_4\right) = 0. \quad (5.8)$$

This yields the equation

$$\left[h_0 + h_2\right]\left[\cot\theta P_2'(\cos\theta) - P_2''(\cos\theta)\right] = 0 \quad \forall r, \theta. \quad (5.9)$$

From this follows the relation between h_2 and h_0

$$h_2 = -h_0. \quad (5.10)$$

Next, we look at $\tilde{G}^2_3$. As the Energy-Momentum-Tensor $\tilde{T}^{\mu}_{\nu}$ is diagonal, the right side of the Einstein Field Equation is zero. This equation can be solved to yield

$$k' = -h_0' - 2h_0\nu. \quad (5.11)$$

Lastly, we add the components that we subtracted in the first step

$$\tilde{G}^3_3 + \tilde{G}^4_4 = -8\pi\left(\tilde{T}^3_3 + \tilde{T}^4_4\right) \quad (5.12)$$

and subtract the part of $\mathcal{O}(\alpha^0)$ that is solved by the TOV Equations. This yields an expression for the pressure perturbation

$$\delta p(r,\theta) = -\frac{e^{-2\lambda} h_0 P_2(\cos\theta)[\lambda' + \nu']}{8\pi r}. \tag{5.13}$$

Using these relations, we can subtract

$$\tilde{G}_1^1 - \tilde{G}_2^2 = -8\pi\left(\tilde{T}_1^1 - \tilde{T}_2^2\right) \tag{5.14}$$

and again, eliminate the terms of order $\mathcal{O}(\alpha^0)$. This yields the differential equation for h_0, we were looking for:

$$h_0'' + h_0'\left(\frac{2}{r} + \nu' - \lambda'\right) + h_0\left(\frac{3\lambda'}{r} + \frac{7\nu'}{r} + 2\nu'' + \frac{\epsilon'[p(r)]}{r}(\lambda' + \nu') - \frac{6e^{2\lambda}}{r^2} - 2\nu'^2 - 2\nu'\lambda'\right) = 0 \tag{5.15}$$

Together with the TOV Equations this ODE can be integrated numerically. Later we will get back to that result.

Exterior Equation for h_0

Outside the star, the pressure and energy density are zero, also λ is equal to ν but with an opposite sign (see Sec. 2.2.4). This reduces (5.15) to

$$h_0'' + h_0'\left(\frac{2}{r} - 2\lambda'\right) - h_0\left(\frac{6e^{2\lambda}}{r^2} + 4\lambda'^2\right) = 0. \tag{5.16}$$

Applying the substitution $x = (r/M_* - 1)$ brings above equation in the form of an Associated Legendre Equation with $\ell = m = 2$ [27]. The general solution to this equation is a superposition of the Associated Legendre Functions $P_2^2(x)$ and $Q_2^2(x)$ [27]:

$$\begin{aligned} h_0(r) &= c_1 Q_2^2\left(\frac{r}{M_*} - 1\right) + c_2 P_2^2\left(\frac{r}{M_*} - 1\right) \\ &= c_1\left(\frac{r}{M_*}\right)^2\left(1 - \frac{2M_*}{r}\right)\left[-\frac{M_*(M_* - r)(2M_*^2 + 6M_* r - 3r^2)}{r^2(2M_* - r)^2}\right. \\ &\quad \left. + \frac{3}{2}\log\left(\frac{r}{r - 2M_*}\right)\right] + 3c_2\left(\frac{r}{M_*}\right)^2\left(1 - \frac{2M_*}{r}\right), \end{aligned} \tag{5.17}$$

where we changed the variables back to r and substituted the expressions for the Legendre Functions.

Determining the Constants

The time component of the metric outside the star can be expanded in the so called buffer zone [4, 24]:

$$\begin{aligned} -\frac{1 - \tilde{g}_{00}}{2} &= -\frac{M_*}{r} - \frac{3\mathcal{Q}_{ij}}{2r^3}\left(\frac{x^i}{r}\frac{x^j}{r} - \frac{1}{3}\delta_{ij}\right) + \mathcal{O}\left(\frac{1}{r^3}\right) + \frac{1}{2}\mathcal{E}_{ij}x^i x^j + \mathcal{O}\left(r^3\right) \\ &= -\frac{M_*}{r} - \frac{\mathcal{Q}}{r^3}P_2(\cos\theta) + \frac{\mathcal{E}}{3}r^2 P_2(\cos\theta) + \mathcal{O}\left(r^{-4}, r^3\right). \end{aligned} \tag{5.18}$$

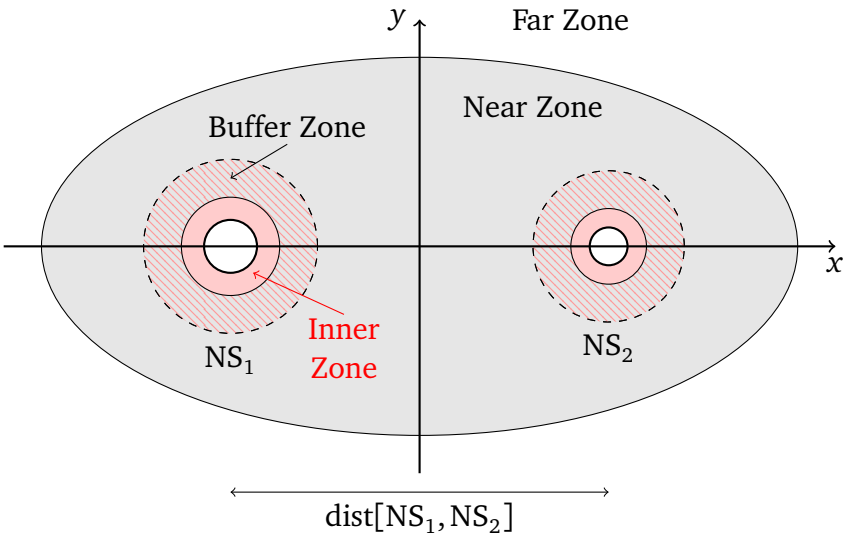

Figure 5.1: Depiction of the zones around the NS. Created on basis of [28].

The buffer zone is the region, where the inner zone and the near zone overlap (see Fig. 5.1), i.e. far away from the star (i.e. $r \gg R_*$) but still not near the companion star (i.e. $r \ll \text{dist}[\text{NS}_1, \text{NS}_2]$) [4]. In this region both the inner zone and the near zone solution are valid. Further information on the various zones around NS binaries can be obtained from [28, 29]. After inserting the ansatz of the exterior solution (5.17) and the exterior expressions for λ and ν into the time component of the metric and expanding at large radii, we can compare this expansion with (5.18). This yields equations for $c_{1/2}$:

$$\frac{8c_1 M_*^3 P_2(\cos\theta)}{5r^3} = -\frac{\mathcal{Q}}{r^3} P_2(\cos\theta) \quad \Rightarrow \quad c_1 = \frac{5\mathcal{E}\lambda_{(\text{tid})}}{8M_*^3} \tag{5.19a}$$

$$\frac{3c_2}{M_*^2} P_2(\cos\theta) = \frac{1}{3}\mathcal{E} P_2(\cos\theta) \quad \Rightarrow \quad c_2 = \frac{M_*^2 \mathcal{E}}{9}. \tag{5.19b}$$

Now that the exterior solution of h_0 is fully determined, we are ready to write out an expression for the Tidal Love Number k_2.

Expression for the Tidal Love Number

We require continuity of h_0 and its derivative at the star's surface:

$$h_0^{(\text{int})}(R_*) = h_0^{(\text{ext})}(R_*) \quad \text{and} \quad h_0'^{(\text{int})}(R_*) = h_0'^{(\text{ext})}(R_*). \tag{5.20}$$

After substitution of $y = R_* h_0'(R_*) \big/ h_0(R_*)$ and the compactness $C = M_*/R_*$ we obtain an expression for k_2:

$$\begin{aligned} k_2 = {} & 8\,(1-2C)^2\, C^5\, [2-2C+(2Cy-y)] \\ & \times \left\{ 10C\left[4C^4+6C^3-22C^2+15C-3\right] y + 4C^4 y - 4C^3 y + 26C^2 y - 24Cy + 6y \right. \\ & \left. + 3\,(1-2C)^2\,[2-2C+(2Cy-y)]\,\log(1-2C) \right\}^{-1} \end{aligned} \tag{5.21}$$

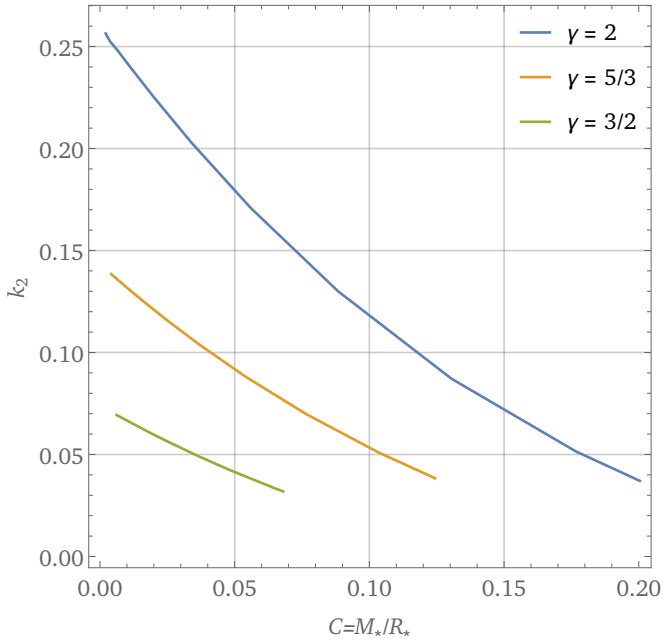

Figure 5.2: Tidal Love Number k_2 plotted over the compactness $C = M_*/R_*$ for polytropes with $\gamma \in \{2, 5/3, 3/2\}$. Only stars that are stable are plotted.

This result agrees with [24, 3, 4]. The coefficient y is determined by the interior solution at $r = R_*$. The solution to (5.15) can be obtained by integrating numerically using the TOV Equations. First however, we need to find boundary conditions for h_0.
The perturbation function h_0, as a component of the metric, should be finite in the center of the star. In order to cancel r in the denominator of the coefficient of h_0 in (5.15), we make the ansatz $h_0 = cr^2$. As (5.15) is arbitrarily scalable and we are only interested in the ratio of h_0 and its derivative, we can set c to one. The boundary conditions therefore are $h_0(r_0) = r_0^2$ and $h_0'(r_0) = 2r_0$. In [24], the expansion up to $\mathcal{O}(r^4)$ is done. The numerical results however are almost identical.

5.3 Numerical Results

In this section we will present numerical results for the Tidal Love Number k_2, derived in the last section, for the polytropic and realistic EoS introduced in Ch. 3.

5.3.1 Polytropic Equations of State

The Tidal Love Number over the compactness C for various polytropic EoS is shown in Fig. 5.2. Only stars that are stable (see Sec. 3.3) are shown. The Love Number measures how easily the star can be deformed. If most of the star's mass is concentrated in the center of the star, the tidal deformation will be smaller. For polytropic EoS the polytropic index determines the stiffness of the EoS. Polytropes with a higher polytropic index are stiffer. For a soft polytrope (i.e. low polytropic index) the matter is mostly in the stars center. Therefore the Tidal Love Number increases with the polytropic index. Stiffer EoS produce stars that are easier to deform [3]. Also the Tidal Love Number decreases with increasing compactness. Compact stars are bound stronger.

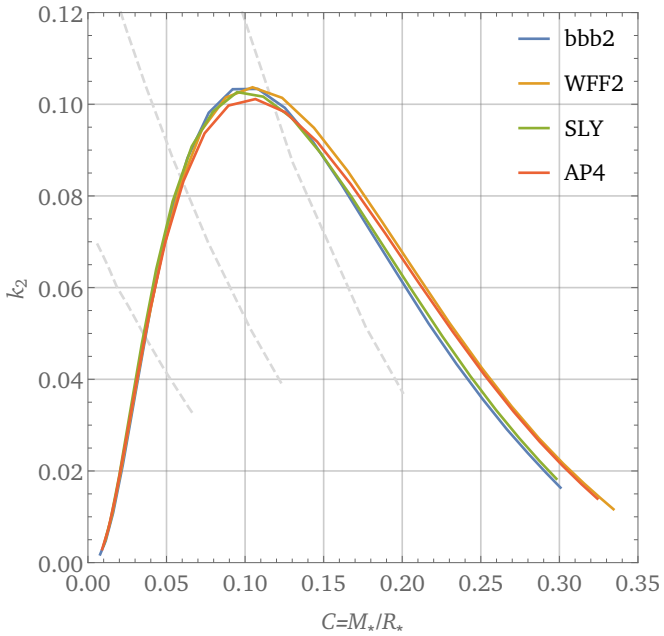

Figure 5.3: Tidal Love Number k_2 plotted over the compactness $C = M_*/R_*$ for realistic EoS. Polytropes with $\gamma \in \{2, 5/3, 3/2\}$ are shown in gray. Only stars that are stable are plotted.

Table 5.1: The central pressure, mass, radius, compactness and the Tidal Love Number of maximum star configurations for various EoS.

EoS	$p_c^{(\max)}[\mathrm{MeV/fm^3}]$	$M_*^{(\max)}[M_\odot]$	$R_*^{(\max)}[\mathrm{km}]$	C	k_2
Poly($\gamma = 2$)	316.228	1.805	12.269	0.217	0.028
Poly($\gamma = 5/3$)	100.000	1.378	15.435	0.132	0.034
Poly($\gamma = 3/2$)	17.783	1.271	25.984	0.072	0.029
bbb2	1000.000	1.923	9.444	0.301	0.016
WFF2	1333.520	2.199	9.710	0.334	0.012
SLY	749.890	2.049	10.149	0.298	0.018
AP4	1000.000	2.212	10.078	0.324	0.014

5.3.2 Realistic Equations of State

In Fig. 5.3 the Tidal Love Number over the compactness for the realistic EoS from Ch. 3 is shown. Furthermore the curves that resulted for polytropes are shown in gray. For large compactness the realistic EoS behave similar to polytropes. For smaller compactness the star's crust gets bigger. This results in smaller values for k_2 [3]. Just as for the polytropes, the realistic EoS Love Number tends to zero as the compactness grows. From (5.21) we see that for the compactness of a BH ($C = 0.5$), the Love Number vanishes, regardless of the EoS that is incorporated in the parameter y [3]. However, there is no physical central density that would lead to a BH formation, so the sequence of stars considered will converge towards zero [4]. For all the EoS, considered in this work, important quantities of the maximum mass stars are listed in Tab. 5.1. These maximum mass stars have a high compactness and therefore a relatively small Love Number, they deliver a perfect compromise between radius and density, while being stable. Stars with maximum k_2 have $M \approx 0.8\, M_\odot$.

Chapter 6

I-Love-Relations

In the last two chapters we dealt with the moment of inertia for a slowly rotating star and the Tidal Love Number, i.e. the deformation of a star by a companion star. With the numerical solutions in hand, we can now focus our attention to the relation between those quantities.
It turns out that the moment of inertia over the Tidal Love Number behaves in a very similar way for any EoS. The relations are EoS independent to within $\mathcal{O}(1\%)$ [4]. This means that the relationship between those quantities does not depend on the NS internal structure. This strongly hints a universal relation between these quantities. Before taking a look at the plot, we define two dimensionless quantities:

$$\bar{\lambda}_{(\mathrm{tid})} \equiv \frac{\lambda_{(\mathrm{tid})}}{M_*^5} = \frac{2}{3} k_2 C^{-5}, \tag{6.1}$$

$$\bar{I} \equiv \frac{I}{M_*^3}. \tag{6.2}$$

In Fig. 6.1, $\bar{I}$ is plotted over the dimensionless $\bar{\lambda}_{(\mathrm{tid})}$ for all EoS considered in this work. The central pressure or equivalently the compactness varies along the curve. As the NS compactness increases, i.e. the Tidal Love Number decreases, the I-Love-Relations for the different EoS converge to a limiting value. This happens, as the compactness gets closer to the compactness of a BH ($C = 0.5$). In the last chapter, we already worked out that the Tidal Love Number approaches zero, as C goes to 0.5, while the moment of inertia $\bar{I}$ tends towards 4 [30]. The BH limit can not be reached, as it is not possible to construct a BH solution by increasing the central pressure of a NS solution by a finite amount [4].
In [4] two possible explanations for such universal relations are discussed: all realistic EoS approach each other far away from the core. The relations may most sensitively depend on the internal structure far away from the core. Furthermore the I-Love-Relations approach the values for a BH that does not have any internal structure dependence.
Further discussion of the I-Love-Relations can be found in e.g. [4, 31].

In [2], experimental upper boundaries for $\bar{\lambda}_{(\mathrm{tid})}$ are presented. For slowly rotating stars of mass $1.4\,M_\odot$, the quantity $\bar{\lambda}_{(\mathrm{tid})}$ is ≤ 800 according to [2]. For the polytrope with $\gamma = 2$, the value for this quantity is more than three times higher than experimentally predicted. This underlines that the polytropes are not very realistic EoS. For the other polytropes considered, the stars with $1.4\,M_\odot$ are unstable. The realistic EoS all agree with the experimental boundary. For all realistic EoS considered in this work, $\bar{\lambda}_{(\mathrm{tid})}(1.4\,M_\odot)$ lies between 200 and 320.

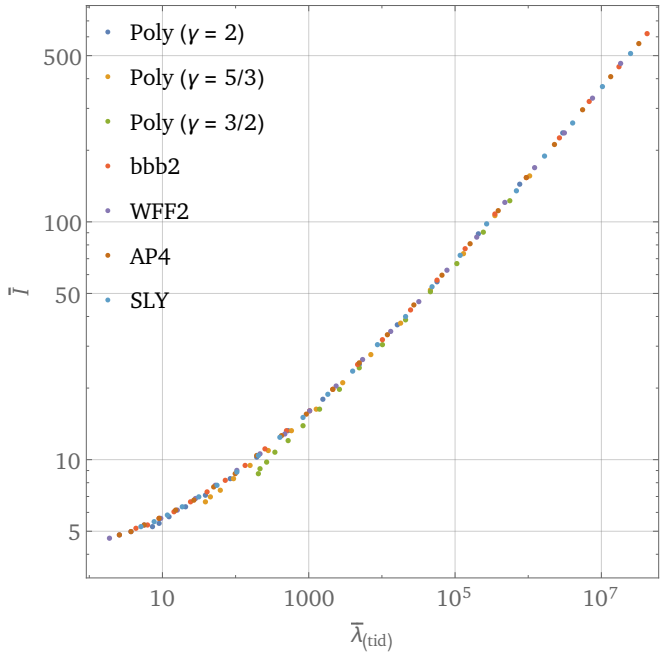

Figure 6.1: Dimensionless moment of inertia $\bar{I}$ over the dimensionless quantity $\bar{\lambda}_{(\mathrm{tid})} \propto k_2$. For all EoS considered in this work. As the compactness increases, $\bar{\lambda}_{(\mathrm{tid})}$ decreases.

Chapter 7

Conclusion and Outlook

In this thesis the Tidal Love Number as well as the I-Love-Relations for NS were calculated. First we introduced the theoretical framework of GR and derived the TOV Equations. Furthermore the ISS was discussed as an analytical solution to the TOV Equations. In the next chapter we solved the TOV Equations for polytropic EoS as well as realistic, tabled EoS. The results for the pressure-radius-curves and the internal mass-radius-curves were presented and discussed. Then the mass-radius-curves for different EoS were calculated and discussed and a stability condition for a NS of a certain mass-radius-configuration was discussed. In the next chapter we focused our attention on the moment of inertia which was derived and computed for the EoS mentioned above. The derivation was done by introducing a perturbation to the metric proportional to a perturbation function $\omega(r)$. Through continuity conditions the exterior and interior solutions for the perturbation function were matched which resulted in an expression for the moment of inertia. We found that the moment of inertia grows with the compactness and that stiffer EoS produce higher values for I. In the following chapter the Tidal Love Number was derived. The derivation was done similarly to the derivation of the moment of inertia. We found that the Tidal Love Number decreases with the compactness, but increases with C for small values and realistic EoS. Lastly we found with the I-Love-Relations that the moment of inertia plotted over the Tidal Love Number is almost independent of the EoS which hinted a universal relation between these quantities.

There is a variety of further research possibilities. As a first step, it could be interesting to calculate the Tidal Love Number for a larger variety of EoS. Calculations for more realistic, tabulated EoS, including some of the EoS discussed in this work, can be found in e.g. [3]. For further investigation it would also be interesting to calculate the star's spin-induced quadrupole moment and the Rotational Love Number. As discovered in [4] these quantities also fulfill universal relations, the I-Love-Q-Relations, i.e. the quadrupole moment over the Tidal Love Number, as well as the quadruple moment over the moment of inertia and the rotational over the tidal Love Number are independent of the EoS. Also it would be interesting to further investigate the reasons for the appearance of such universal relations. The I-Love-Q-Relations open the door to even further use of gravitational wave observation. Measuring only one of I-Love-Q quantities automatically results in knowledge of the others. Additionally the investigation of possible further universal relations could be interesting.
Another interesting extension to this thesis could be to repeat the calculations for rapidly spinning NS as done in e.g. [32]. This however, is more of an academic interest, as for almost all NS that have been astrophysically observed, the spin period is sufficiently long that the slow-rotation expansion is an excellent approximation [4].

Bibliography

[1] Potekhin A. Haensel, P. and D. G. Yakovlev. *Neutron stars 1: Equation of state and structure*, volume 326. Springer Science & Business Media, 2007.

[2] Abbott, B. et al. GW170817: Observation of gravitational waves from a binary neutron star inspiral. *Physical Review Letters*, 119(16):161101, 2017.

[3] T. Hinderer, B. D. Lackey et al. Tidal deformability of neutron stars with realistic equations of state and their gravitational wave signatures in binary inspiral. *Physical Review D*, 81(12):123016, 2010.

[4] K. Yagi and N. Yunes. I-Love-Q relations in neutron stars and their applications to astrophysics, gravitational waves, and fundamental physics. *Physical Review D*, 88(2):023009, 2013.

[5] S. DeDeo and D. Psaltis. Towards new tests of strong-field gravity with measurements of surface atomic line redshifts from neutron stars. *Physical review letters*, 90(14):141101, 2003.

[6] R. Kippenhahn, A. Weigert, and A. Weiss. *Stellar structure and evolution*, volume 192. Springer, 1990.

[7] A. Einstein. Erklärung der Perihelbewegung des Merkur aus der allgemeinen Relativitätstheorie. *Sitzungsberichte der Königlich Preussischen Akademie der Wissenschaften*, 47(2):831–839, 1915.

[8] A. Einstein. Die Feldgleichungen der Gravitation. *Sitzungsberichte der Königlich Preussischen Akademie der Wissenschaften*, 47(2):744–847, 1915.

[9] A. Einstein. Zur allgemeinen Relativitätstheorie. *Sitzungsberichte der Königlich Preussischen Akademie der Wissenschaften*, 47(2):799– 801, 1915.

[10] Prof. Dr. J. Wambach. *Scriptum: Allgemeine Relativitätstheorie*. WS 2013/2014.

[11] N. K. Glendenning. *Compact stars: Nuclear physics, particle physics and general relativity*. Springer Science & Business Media, 2012.

[12] K. Schwarzschild. Über das Gravitationsfeld eines Massenpunktes nach der Einsteinschen Theorie. *Sitzungsberichte der Königlich Preussischen Akademie der Wissenschaften*, 7:189–196, 1916.

[13] K. Schwarzschild. Über das Gravitationsfeld einer Kugel aus inkompressibler Flüssigkeit. *Sitzungsberichte der Königlich Preussischen Akademie der Wissenschaften*, 1:424, 1916.

[14] N. Rohr J. Heinzle and C. Uggla. Spherically symmetric relativistic stellar structures. *arXiv preprint gr-qc/0304012*, 2003.

[15] LORENE Software Library. https://lorene.obspm.fr.

[16] K. Schertler C. Greiner and J. Schaffner-Bielich et al. Quark phases in neutron stars and a third family of compact stars as signature for phase transitions. *Nuclear Physics A*, 677(1-4):463–490, 2000.

[17] Xtreme Group at the University of Arizona. http://xtreme.as.arizona.edu/NeutronStars/, (Checked: March 2019).

[18] F. Özel and D. Psaltis et al. The dense matter equation of state from neutron star radius and mass measurements. *The Astrophysical Journal*, 820(1):28, 2016.

[19] F. Douchin and P. Haensel. *Astron. Astrophys.*, 380:151, 2001.

[20] I. Bombaci M. Baldo and G.F. Burgio. *Astron. Astrophys.*, 328:274, 1997.

[21] V. Fiks R. B. Wiringa and A. Fabrocini. *Phys. Rev. C*, 38:1010, 1988.

[22] V. R. Pandharipande A. Akmal and D. G. Ravenhall. Equation of state of nucleon matter and neutron star structure. *Phys. Rev. C*, 58:1804, 1998.

[23] J. B. Hartle. Slowly rotating relativistic stars. I. Equations of structure. *The Astrophysical Journal*, 150:1005, 1967.

[24] T. Hinderer. Tidal love numbers of neutron stars. *The Astrophysical Journal*, 677(2):1216, 2008.

[25] K. S. Thorne and A. Campolattaro. Non-radial pulsation of general-relativistic stellar models. i. analytic analysis for l>= 2. *The Astrophysical Journal*, 149:591, 1967.

[26] T. Regge and J. A. Wheeler. Stability of a schwarzschild singularity. *Physical Review*, 108(4):1063, 1957.

[27] A. Jeffrey and H. Dai. *Handbook of mathematical formulas and integrals*. Elsevier, 2008.

[28] N. Yunes, W. Tichy, B. J. Owen, and B. Brügmann. Binary black hole initial data from matched asymptotic expansions. *Physical Review D*, 74(10):104011, 2006.

[29] W. L. Burke and K. S. Thorne. Relativity, 1970.

[30] K. S. Thorne, R. H. Price, and D. A. Macdonald. Black holes: the membrane paradigm. *Yale University Press*, 1986.

[31] T. Gupta, B. Majumder, K. Yagi, and N. Yunes. I-Love-Q relations for neutron stars in dynamical Chern Simons gravity. *Classical and Quantum Gravity*, 35(2):025009, 2017.

[32] E. Berti and N. Stergioulas. Approximate matching of analytic and numerical solutions for rapidly rotating neutron stars. *Monthly Notices of the Royal Astronomical Society*, 350(4):1416–1430, 2004.

Acknowledgments

First of all I would like thank Priv.-Doz. Dr. Michael Buballa for giving me the opportunity to work on this exciting topic and for the time he took during my project. Furthermore, I want to thank all members of the NHQ-Group for their interesting talks during the group meetings.
Especially I want to express my deep thankfulness to Martin Steil. His incredible technical expertise, but especially his courteous helpfulness at any time, made this work in its current shape possible. Additionally I want to thank him for the second assessment of the thesis.
Also I would like to thank my good friend Timo Velten for correcting grammatical mistakes of an earlier version of this work. Last but not least I want to thank my friends, my girlfriend Deborah Engesser and my family for their support during my studies.

Danksagungen

Zuerst möchte ich mich bei Priv.-Doz. Dr. Micheal Buballa für die Möglichkeit bedanken, mich mit diesem spannenden Thema zu beschäftigen und für die Zeit, die er während meines Projektes aufgewendet hat. Weiterhin möchte ich mich bei allen Mitgliedern der NHQ-Gruppe für die interessanten Vorträge im Rahmen des Gruppentreffens bedanken.
Mein ganz besonderer Dank gilt Martin Steil. Seine unglaubliche fachliche Expertise, aber besonders seine zuvorkommende Hilfsbereitschaft zu jeder Zeit, machte diese Arbeit in ihrer derzeitigen Form möglich. Desweiteren bin ich ihm sehr dankbar, dass es sich bereit erklärte, das zweite Gutachten zu übernehmen.
Auch möchte ich mich bei meinem guten Freund Timo Velten für die Korrektur grammatikalischer Fehler bedanken. Zu guter letzt möchte ich mich bei meinen Freunden, meiner Freudin Deborah Engesser und meiner Famile für die Unterstützung während meines Studiums bedanken.